J. Fluid Mech. (1982), *vol.* 116, *pp.* 31–57
Printed in Great Britain

Coherence between large-scale jet-mixing structure and its pressure field

By M. R. DAVIS

School of Mechanical and Industrial Engineering,
University of New South Wales, Kensington, NSW 2033, Australia

(Received 19 April 1980 and in revised form 7 July 1981)

A schlieren system has been arranged to sense the total fluctuation over a cross-section of the flow and thus becomes very sensitive to large-scale azimuthally coherent structures in the flow. For a natural unexcited jet it is found that there is a concentration of the large-scale structure at a characteristic Strouhal number which is not sensitive to the beam thickness and which reduces progressively with distance from the nozzle. This large-scale structure exhibits a coherence of over 70 % with the near-field pressure and convects at between 75 % and 95 % of the jet velocity. The coherence between the potential core-pressure field and the large-scale structure downstream increases rapidly with distance from the nozzle exit plane, rather limited coherence being found at the exit plane for these observations at a jet-exit Mach number $M_j = 0{\cdot}7$. Movement of a central microphone from $x = 0$ to $x = 2D$ introduced a solid centre body over the first 2·5 diameters of flow and gave rise to a set of discrete components in the flow structure in the range $0{\cdot}6 < S < 1{\cdot}4$.

With harmonic excitation at $S = 1{\cdot}12$ a subharmonic at $S = 0{\cdot}55$ occurs at $x/D = 3$ and a second at $S = 0{\cdot}26$, $x/D = 6$. The flow cross-sectional-average sensing thus appears to show up the vortex-pairing mechanism at greater distances from the nozzle than is easily detectable by other means. Under strong impulse excitation a set of discrete components was observed in a transient response extending over times of $400D/U_j$. These had a strongest component which decreases more rapidly in Strouhal number with distance than that associated with natural or harmonically excited conditions.

1. Introduction

Many observations of mixing shear layers and jets have provided strong evidence that the turbulence contains distinctive large-scale structures. For example the photographs of Bradshaw, Ferris & Johnson (1964) and Brown & Roshko (1974) show the presence of large-scale structures in a three-dimensional jet flow and in a two-dimensional mixing layer, respectively. Further, it has been demonstrated that a large-scale vortex-pairing mechanism exists (Winant & Browand 1974) and flow visualization has given good support to this concept in the two-dimensional layer. A similar mechanism has been demonstrated in the initial region of a mixing jet shear layer on the basis of hot-wire signals (for example, Davis & Davies 1979) where the structure is predominantly two-dimensional. Crow & Champagne (1971), on the basis of flow visualization, also identify initial shear-layer ring vortices and at larger

distances distinctive coherent puffs were evident. Moore (1977, and in a personal communication) has also shown that the visual evidence for large-scale disturbances can be enhanced using a near-field microphone array to trigger the photographic system, the motion of the disturbance becoming evident as a time delay is introduced in the trigger signal.

Excitation of the flow in a symmetrical manner, generally from upstream, tends to produce much stronger evidence for large-scale structures. Crow & Champagne (1971), Moore (1977) and Heavens (1978) all provide clear evidence for the influence of excitation, of harmonic or impulse type, in producing strongly ordered structure in the resulting flow. Davies & Yule (1975) and Widnall, Bliss & Tsai (1974) show, however, that such orderly structures as ring vortices can break up into orderly three-dimensional vortices with regular peripheral periodicity.

Whilst flow-visualization studies provide strong evidence that large-scale structures do occur in practice, they are somewhat limited in that a rather subjective interpretation is generally necessary. Some selectivity is involved in choosing a representative result from a set of photographs obtained at different times, and this raises the problem of whether the observed events comprise a significant portion of the total motion. Further, the large-scale structures often exist in the presence of apparently more random structures, or at least fine-scale structures, and it is often difficult to identify the large structure clearly. This is particularly the case at higher Reynolds numbers. More-quantitative resolution of large-scale structures has generally been based on hot-wire or other localized turbulent signals. Approaches here vary from efforts to identify distinctive patterns in the signal from a single location (e.g. Bruun 1977) to the use of sensing arrays to sense regular spatial events (Townsend 1979). However, often the local signals are dominated by the energy of the fine-scale turbulent structure, making the identification of regular large-scale events by this approach more difficult.

In the present work it is intended to develop a simple sensing technique whereby a gross overall signal is obtained from the flow, in the expectation that a spatially averaged time-dependent signal would be more responsive to large-scale spatial structures. This would overcome some of the difficulties associated with conditionally sampled localized turbulent signals on the one hand and of selected instantaneous photographs on the other. In particular, it would offer the opportunity of resolving more easily the large-scale structure in the presence of fine-scale disturbances. Such an approach is essentially a compromise between the use of localized quantitative results and of overall visualizations interpreted subjectively. The particular method selected is that of sensing by a phototransistor the total light transmitted past the knife edge of a conventional schlieren system. The dynamic quantitative use of the schlieren method on the basis of very thin sensing beams has been discussed in detail by Davis (1971, 1972, 1975), where it is shown that the signals at appreciable jet Mach numbers (up to 0·9) are dominated by contributions from the mixing of the jet and surroundings at different density. The scales of the density structure for an unheated compressible jet were found to be similar to those obtained where the mixing process was observed, on the basis of its velocity fluctuations, with hot-wire probes. Winarto (1979) has also shown that, whilst pressure fluctuations do contribute to the schlieren signal, their contribution does not dominate over that due to mixing even when a jet of significant Mach number is heated so that the temperature gradient across its shear

layer is eliminated. In the present work therefore, using an unheated jet, the schlieren is sensing the mixing process and not the pressure structure. In order to maximize the sensitivity of the system to flow structures having axial symmetry the beam was set up (by using a mask) in the form of a thick slab which intercepted the jet axis at right angles. As will be seen, this arrangement greatly enhances the contribution of azimuthally coherent components of the flow structure.

2. The large-aperture dynamic schlieren sensing system

2.1. *Experimental apparatus*

The experimental observations to be described were carried out using a 1·27 cm diameter nozzle operated at a Mach number of 0·7, with a flow stagnation temperature equal to the ambient temperature of the surrounding air, and Reynolds number based on its diameter of $2{\cdot}3 \times 10^5$. The test nozzle was located centrally and discharging upwards in a small anechoic chamber with sides and height of 2·5 m. Extraneous noise from the supply compressor was eliminated from the observations by high-pass filtering signals at 200 Hz using a Krohn–Hite filter. This noise was due mainly to transmission through the chamber walls and was some 30 dB below the total sound-pressure level produced by the jet within the chamber. Moreover, it lay in the low-frequency range below 200 Hz and it was quite negligible after filtering. Operation of the system without the nozzle and contraction in place but with the flow on demonstrated that noise propagating through the delivery pipework was also negligible. Control of the jet was by a weak throttle to the compressor inlet, so that no choked valve controls were located in the supply pipework.

Two plenum chamber configurations were used, as shown in figure 1. The first (figure 1*a*) incorporated a spark source to provide impulse excitation; this configuration was also used to make all observations of the natural unexcited jet, and incorporated honeycomb and gauze screens to smooth the flow into the final contraction (area ratio 36:1). The spark was driven by the discharge of a 10 kV capacitor. The second configuration (figure 1*b*) incorporated a Kerry ultrasonic horn and driver unit to provide harmonic excitation of the jet at 20 kHz.

The schlieren system comprised a conventional incandescent light illuminating a slit source and providing a parallel beam of light from a spherical mirror of diameter 10·2 cm. Care was taken to ensure that the intensity of the beam was uniform by phototransistor observation, and the slit was adjusted to an opening of 0·31 mm. As discussed by Davis (1971), this would provide a sensitivity at the schlieren knife edge corresponding to a full-scale angular deflection range of 3×10^{-4} rad due to the flow from a second 104 cm focal length mirror used to focus the beam to the knife edge. According to Davis (1971) this range would be sufficient to encompass unsteady deflections due to the turbulent jet flow so that the system would have a linear response to flow fluctuations. A sensing phototransistor was placed immediately behind the knife edge, and included a lens in its face so that it effectively sensed the total light from the whole schlieren beam passing the knife edge.

A masking plate with a variable and moveable opening was inserted to block the schlieren beam immediately before it intercepted the flow. By adjusting the mask opening, only a small slab segment of the original beam passed the flow and was sensed by the phototransistor. Thus the phototransistor output represented the

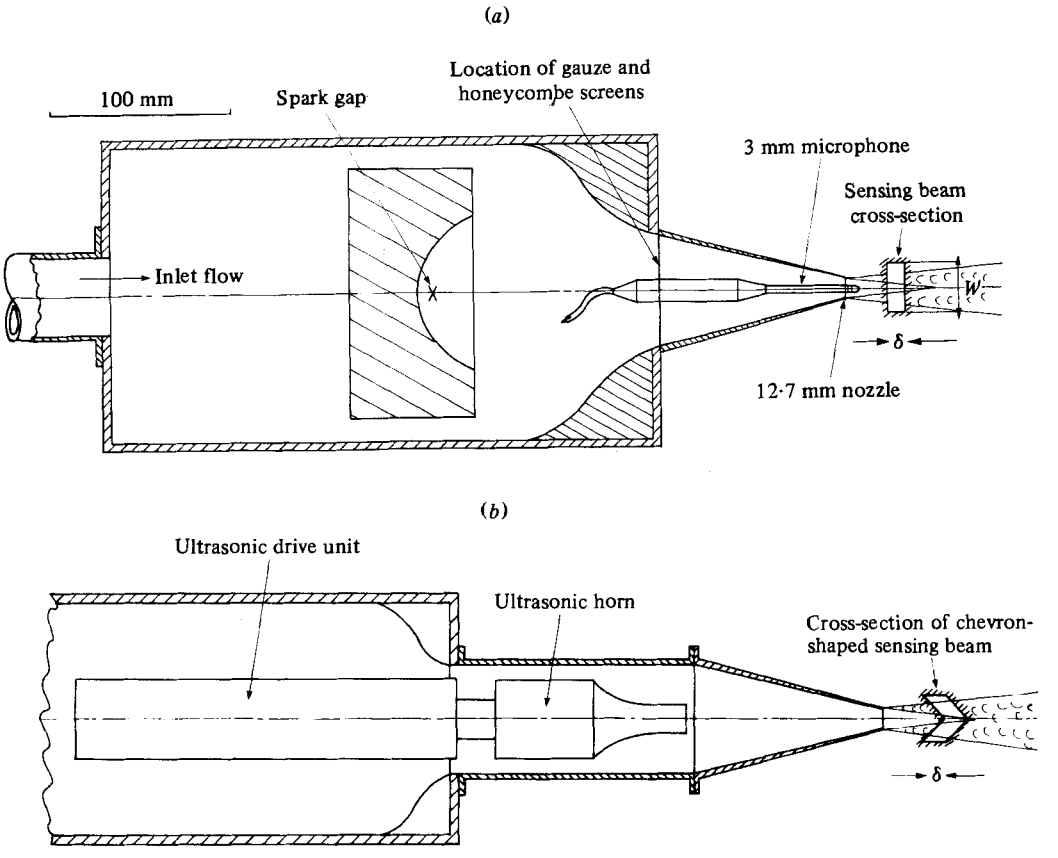

FIGURE 1. Configuration of nozzle and plenum for experimental tests. (*a*) Arrangement for natural jet and impulsively excited jet. (*b*) Arrangement for harmonically excited jet. (Central microphone only in place when observing potential core pressure; all dimensions to scale.)

unsteady signal integrated over the slab within the flow. The cross-section of this sensing beam is shown in figure 1 (*a*) against the jet flow, a width of $W/D = 2$ being used to sense a complete thick slice of the jet at right angles to its axis. For most of the present observations the thickness δ of the sensing slab beam was set to $\frac{1}{8}$ of its distance from the nozzle, as discussed below. Some observations were also made with a chevron-shaped opening in the mask, as illustrated in figure 1 (*b*).

The acoustic pressure field of the jet was observed using Bruel and Kjaer condenser microphones, a 3 mm microphone being used in the near field and a 13 mm microphone in the far field. The latter was mounted on a circular arc traverse at a distance of 50 nozzle diameters from the nozzle exit. Direct measurements of the schlieren phototransistor output and of sound-pressure fluctuations were made using a Bruel and Kjaer type 2107 measuring amplifier, which was used to record intensity values and some narrow band (6 % bandwidth filter) spectra. The majority of spectrum and co-spectrum functions were obtained by tape-recording the signals using a Racal Thermionic FM recorder, and subsequently replaying the signals through a Hewlett Packard Digital Signal Analyzer type 5420A. Output from the latter was via a digital *x-y* plotter. The maximum overall bandwidth of this system was 25 kHz, allowing observations to a maximum Strouhal number of 1·4.

2.2. *Response of the schlieren slab beam*

The sensing of turbulence by a schlieren pencil beam passing through a turbulent flow has been discussed in detail by Davis (1971, 1972, 1975), and the response of a schlieren slab beam will now be discussed along broadly similar lines. The fluctuating output E_s of the slab beam in response to the density gradient $\partial\rho/\partial x$ within the flow (with cross-sectional co-ordinates r and θ, and x the distance from the nozzle exit) is

$$E_s = A\int_0^{2\pi}\int_0^R\int_{x_1}^{x_2}\frac{\partial\rho}{\partial x}r\,dr\,d\theta\,dx, \tag{1}$$

where A is a constant embodying the refractive-index parameter (Gladstone–Dale constant) and the photosensor sensitivity to angular deflections. For a small variation δ between x_1 and x_2 this becomes

$$E_{s\delta} = A\delta\int_0^{2\pi}\int_0^R\frac{\partial\rho}{\partial x}r\,dr\,d\theta, \tag{2}$$

where $\delta = x_2 - x_1$, the beam thickness. It follows that the root-mean-square amplitude of the observed fluctuation then increases in proportion to δ. However, if δ becomes sufficiently large that $\partial\rho/\partial x$ is not effectively constant over the thickness of the slab ($x_1 < x < x_2$) for given (r,θ) then we have

$$E_{s\delta} = A\int_0^{2\pi}\int_0^R\int_{x_1}^{x_1+\delta}\frac{\partial\rho}{\partial x}r\,dr\,d\theta\,dx = A\int_0^{2\pi}\int_0^R[\rho(x_1+\delta)-\rho(x_1)]\,r\,dr\,d\theta. \tag{3}$$

The unsteady deflection intensity thus becomes (where the overbar denotes time average)

$$I_{s\delta} = A^2\int_0^{2\pi}\int_0^{2\pi}\int_0^R\int_0^R\overline{[\rho_{r\theta}(x_1+\delta)\,\rho_{r'\theta'}(x_1+\delta)+\rho_{r\theta}(x_1)\,\rho_{r'\theta'}(x_1)]}\,rr'\,dr\,d\theta\,dr'\,d\theta', \tag{4}$$

provided that the separation δ is sufficiently large that the fluctuations at the two sides of the slab beam are not correlated, i.e. provided that δ appreciably exceeds the streamwise integral scale. If the flow is homogeneous over the distance δ, then conditions at both faces of the slab beam are similar and

$$I_{s\delta} = 2A^2\int_0^{2\pi}\int_0^{2\pi}\int_0^R\int_0^R\overline{\rho_{r\theta}\rho_{r'\theta'}}\,rr'\,dr\,d\theta\,dr'\,d\theta'. \tag{5}$$

This result is thus independent of δ. Figure 2 shows the variation of the output of the large schlieren as a function of the beam thickness. For small thicknesses the output increases in proportion to the sensing-beam thickness, as indicated by (2), whilst for larger beam thicknesses the output approaches a nearly constant value, as indicated by (5). These results were used as a basis for selecting a beam thickness which was large enough to give an output independent of beam thickness (equation (5)) and yet small enough to provide relatively localized indications of the structure at different sections along the jet axis. For the results shown at $x/D = 5$, a beam thickness of $\delta = 0{\cdot}6D$ would be the minimum which would meet these requirements, giving an output within 2·5 % of the maximum for large δ, and accordingly it was decided to operate the schlieren with a beam thickness $\delta = \frac{1}{8}x$. It should be borne in mind that the structural scales of the growing shear layer increase in proportion to x (Davis 1975) and therefore the sensing-beam thickness was also increased in proportion to x.

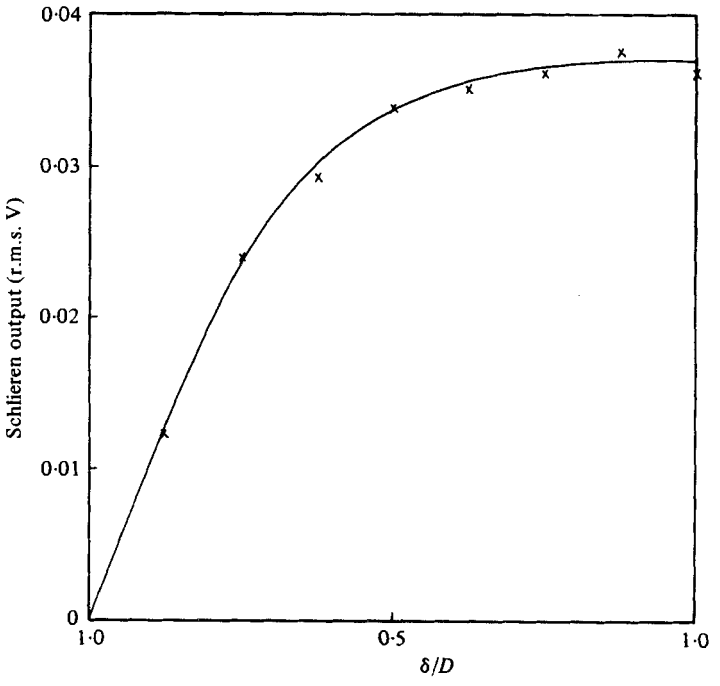

FIGURE 2. Increase of schlieren slab-beam output with beam thickness (x/D = 5, natural jet).

The response of the schlieren in the presence of flow structures which are azimuthally coherent can be demonstrated by putting $\rho_{r\theta} = \rho_{cr} + \rho_{ir\theta}$ where ρ_{cr} denotes an azimuthally coherent disturbance which may depend only upon r, and $\rho_{ir\theta}$ denotes an azimuthally incoherent component. The system output thus becomes

$$I_{s\delta} = 2A^2 \int_0^{2\pi}\int_0^{2\pi}\int_0^R\int_0^R \overline{(\rho_{cr}+\rho_{ir\theta})(\rho_{cr'}+\rho_{ir'\theta'})}\, rr'\, dr\, d\theta\, dr'\, d\theta'$$

$$= 8\pi^2 A^2 \int_0^R\int_0^R \overline{\rho_{cr}\rho_{cr'}}\, rr'\, dr\, dr' + 2A^2 \int_0^{2\pi}\int_0^{2\pi}\int_0^R\int_0^R \overline{\rho_{ir\theta}\rho_{ir'\theta'}}\, rr'\, dr\, d\theta\, dr'\, d\theta', \qquad (6)$$

if the incoherent and coherent components are independent (as they must be). Thus the schlieren will respond to both coherent and incoherent components. The relative magnitude of the two components can be estimated approximately in terms of representative mean-square magnitudes of each, $\overline{\rho_c^2}$ and $\overline{\rho_i^2}$, say. For an annular shear layer which is not thick by comparison with its radius R_L, the beam intensity becomes

$$I_{s\delta} \sim R_L^2\, 8\pi^2 A^2 \int \overline{\rho_c^2} l_{cr}\, dr + 2A^2 R_L \int_0^{2\pi}\int_{\text{layer}} \overline{\rho_i^2} l_{ir} l_{i\theta}\, dr\, d\theta, \qquad (7)$$

where l_{cr}, l_{ir} and $l_{i\theta}$ denote a radial integral scale of the coherent structure and radial and azimuthal integral scales of the incoherent structure, respectively, and are given by integrals of correlation functions

$$l_{cr} = \int \frac{\overline{\rho_{cr}\rho_{cr'}}}{\overline{\rho_c^2}}\, dr', \quad l_{ir} = \int \frac{\overline{\rho_{ir}\rho_{ir'}}}{\overline{\rho_i^2}}\, dr', \quad l_{i\theta} = \int \frac{\overline{\rho_{i\theta}\rho_{i\theta'}}}{\overline{\rho_i^2}}\, r\, d\theta'. \qquad (8)$$

For a typical mixing layer (see for example Davis 1975) integral scales of fine-scale-dominated incoherent turbulence would be expected to vary as $l \sim 0{\cdot}05x$ whilst the layer thickness varies as $t \sim 0{\cdot}2x$. If $l_{cr} \sim O(t)$, i.e. the coherent structure spans the entire shear layer, then we see that the ratio of the two contributing terms to the large-aperture schlieren signal is estimated by (R_L = layer mean radius)

$$\frac{\text{coherent component}}{\text{incoherent component}} = 320\pi^2\left(\frac{R_L}{x}\right)\frac{\overline{\rho_c^2}}{\overline{\rho_i^2}}.$$

At the greatest distance considered in the present work, just beyond the end of the smooth potential core of the flow from the nozzle, $x/R_L \simeq 14$ and we see that

$$\frac{\text{coherent component}}{\text{incoherent component}} \geqslant 226\frac{\overline{\rho_c^2}}{\overline{\rho_i^2}}.$$

These estimates thus show how the use of a large-aperture sensing system results in a substantial weighting of several hundred times being introduced, to enhance the coherent-component contribution to the total signal observed. In effect this is caused by the strong sensitivity of area-integrated signals to the scale of disturbances over the area (Davis 1971, 1975). The schlieren system is essentially sensing the total cross-sectional density fluctuations, and these fluctuations are weighted in proportion to their integral area scales.

When spectra of the schlieren are considered it is apparent that the streamwise thickness of the beam may influence the output-signal spectra as there will be an aspect of matching present between the streamwise scale of any particular component with the beam thickness. For a disturbance which moves at a convection speed U_c and has the form

$$\rho(x, r, \theta) = \rho(r, \theta)\left(\frac{x - U_c t}{a}\right)\exp\left(-\left(\frac{x - U_c t}{a}\right)^2\right), \tag{9}$$

the response of the schlieren is

$$E_{sa} = A\int_0^{2\pi}\int_0^R \rho(r,\theta)\,dr\,d\theta\left\{\left(\frac{x+\delta-U_c t}{a}\right)\exp\left(-\left[\frac{x+\delta-U_c t}{a}\right]^2\right)\right.$$
$$\left.-\left(\frac{x-U_c t}{a}\right)\exp\left(-\left[\frac{x-U_c t}{a}\right]^2\right)\right\}. \tag{10}$$

Making an arbitrary shift of origin to $x = 0$, and putting $\delta/a = K$, the ratio of beam thickness to disturbance scale a, and then incorporating the cross-sectional integral into a parameter A_1, the output is

$$E_{sa} = A_1\{(K - \bar{t})\,e^{-(K-\bar{t})^2} + \bar{t}\,e^{-\bar{t}^2}\},$$

where $\bar{t} = U_c t/a$. The total disturbance energy sensed by the beam during the passage of the disturbance is thus, after squaring and integrating,

$$\frac{1}{A_1^2}\frac{U_c}{\delta}\int_{-\infty}^{\infty} E_{sa}^2(t)\,dt = \frac{1}{KA_1^2}\int_{-\infty}^{\infty} E_{sa}^2\,dt = \frac{1}{K}\{1 + e^{-\frac{1}{2}K^2}(K^2 - 1)\}\int_0^{\infty} e^{-2t_1^2}\,dt_1$$
$$= 0{\cdot}632\{1 + e^{-\frac{1}{2}K^2}(K^2 - 1)\}/K. \tag{11}$$

This function is shown in figure 3, and we see that as the disturbance size becomes much larger than the beam thickness so the output becomes very small and tends to

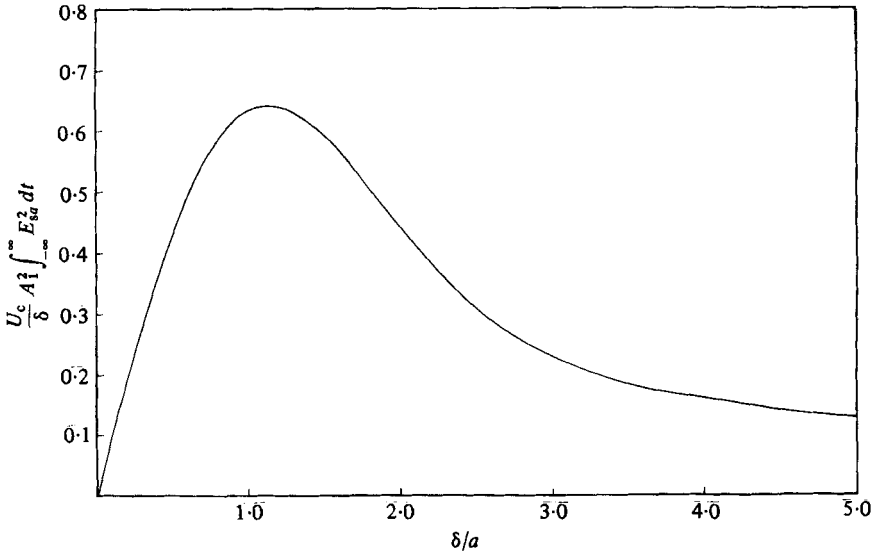

FIGURE 3. Response of finite-thickness sensing beam to a convecting flow disturbance.

zero. Where the disturbance matches the beam thickness the system shows a maximum response at $\delta/a = 1{\cdot}14$. As the disturbance scale decreases further, so the function decreases to zero.

Where a flow contains a distribution of disturbances of differing scale in the x-direction, the spectrum of the output signal depends upon the spectral distribution of the disturbances, their respective cross-sectional coherence, and will be weighted owing to the beam thickness as just discussed. If all disturbances had a similar cross-sectional coherence then the output spectrum of the schlieren would represent the product of this weighting and spectral distribution of the disturbances and we see that at low frequency (i.e. as $a \to \infty$) the observed spectral density should tend to zero. This is shown in figure 4 (a), which shows energy spectra for different sensing-beam thicknesses, all spectral curves reducing at low frequency as expected. It may be seen that the location of the maximum spectral density is not greatly altered as the beam thickness was increased from $\frac{1}{8}D$ to $\frac{9}{8}D$ (D being the nozzle diameter) at the observing position $5D$ from the nozzle exit plane. For the larger beam thickness it is located at $S = fD/U_j = 0{\cdot}346$, whilst at the thinnest beam thickness it is located at $S = 0{\cdot}428$. Thus a ninefold reduction of the beam thickness has resulted in only a 24 % increase in Strouhal number of the spectral maximum. It is concluded therefore that this is a result of a substantial and strongly emphasized component existing in the flow, for had the spectral distributions of the disturbances themselves been relatively uniform and if they all had similar coherence over the cross-section of the flow then it would be expected that, as the response-weighting function of figure 3 changed by a factor of 9 in the parameter δ/a, a similar change would occur in the peak response in the observed spectrum. Whilst the peak in the spectrum is not discrete, it is quite evident that the observed Strouhal number of this maximum is relatively weakly dependent upon the thickness of the sensing beam and suggests that there is a concentration of energy of those disturbances which have higher azimuthal coherence into the range around $S \simeq 0{\cdot}4$ at this particular position in the flow. The spectra of figure 4 (a) otherwise show a general similarity to the form of figure 3, increasing approximately in

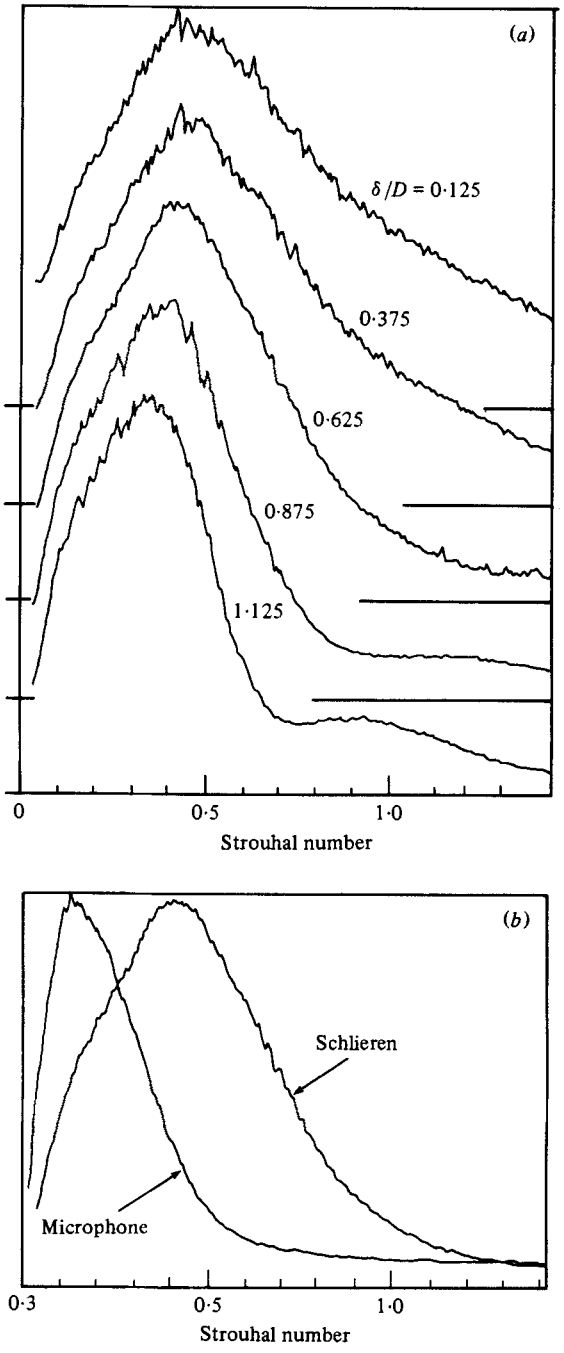

FIGURE 4. (*a*) Comparative spectra of slab schlieren output for different beam thicknesses in a natural jet (vertical axis – spectral density, linear scale $x/D = 5$). (*b*) Comparative spectra of slab schlieren output and adjacent near-field microphone (vertical axis as (*a*), $x/D = 5$, $\delta/D = \frac{5}{8}$, microphone at $y/D = 1{\cdot}75$).

proportion to frequency for small values of frequency (i.e. the large-scale disturbances), and showing a gradual approach to zero at high frequency which is more rapid for the larger values of δ (i.e. where larger values of δ/a apply), as expected from figure 3. However, it appears that the characteristic of this large-aperture sensing system to emphasize very strongly components which are coherent over the flow cross-section implies that the identification of these coherent disturbances in terms of their Strouhal number is not highly sensitive to the particular beam thickness selected. Co-spectra between a near-field microphone and the adjacent schlieren output were also found to be virtually independent of beam thickness, the coherence maximum value remaining close to 70% and at almost the same Strouhal number (0·37) for $\frac{1}{8}D \leqslant \delta \leqslant \frac{9}{8}D$ at $x/D = 5$. These co-spectra are discussed in more detail in §3.1 which follows. Therefore the selection of a suitable beam thickness on the basis of the change of total signal intensity will be adequate for the purpose of identifying azimuthally coherent components in the flow. The schlieren/near-field-pressure coherence in particular is very insensitive to beam thickness.

It may be noted that the spectra obtained using this large-aperture schlieren arrangement differ substantially from the spectra of thin-pencil schlieren beam signals as discussed by Davis (1971), which do not show such a strong concentration of energy within a well-defined range of Strouhal number. This comparison provides further confirmation that the present observations are the result of the high sensitivity of the large-aperture schlieren to azimuthally coherent disturbances and that the flow contains such disturbances in a distinct Strouhal-number range. Figure 4(*b*) compares the spectra of the schlieren signal with that of an adjacent near-field microphone, and it may seem that the two are quite different in distribution, their maxima occurring at $S = 0{\cdot}13$ in the case of the microphone signal and at $S = 0{\cdot}46$ for the large-aperture schlieren. This serves to emphasize the point made in §1 that the schlieren is sensitive to the mixing structure of the flow rather than to its pressure field. Whilst an exact explanation for this difference cannot be attempted at this stage, it is clear that the schlieren is sensing disturbances at a particular cross-section of the jet, whilst the microphone responds to the overall effect of the complete jet on the pressure field. The near pressure field is not only caused by the turbulence at that cross-section. The implication of figure 4 is that stronger but less-coherent (as the following discussion of figure 8 indicates) contributions to the near pressure field come from positions further from the nozzle exit than the schlieren-beam position at $x/D = 5$.

3. Observations of coherent effects between jet structure and pressure field

3.1. *The natural unexcited jet*

Using the plenum-chamber configuration of figure 1(*a*) a series of records were made of microphone and schlieren signals and analysed using the digital signal analyser. Spectra were formed as the average of between 2000 and 5000 Fourier transforms of this record, the larger number of averages being used where coherence between the signals was small to improve resolution. For most of the results, this number of averages led to the dominant uncertainty in the spectra formed being that due to slight unsteadiness in the signal records themselves. This was in turn due to small variations in

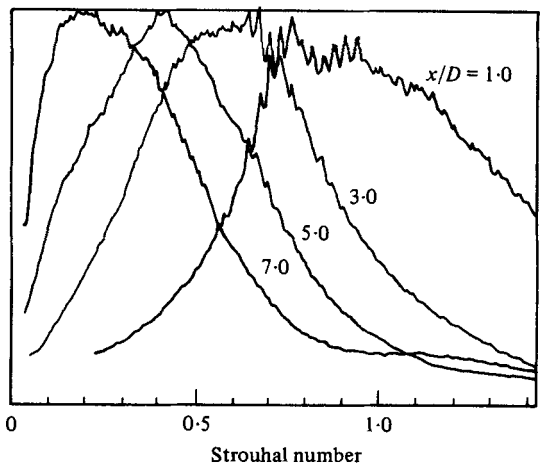

FIGURE 5. Spectra of slab schlieren in the natural jet (vertical axis is spectral density, linear scale $\delta = \frac{1}{8}x$).

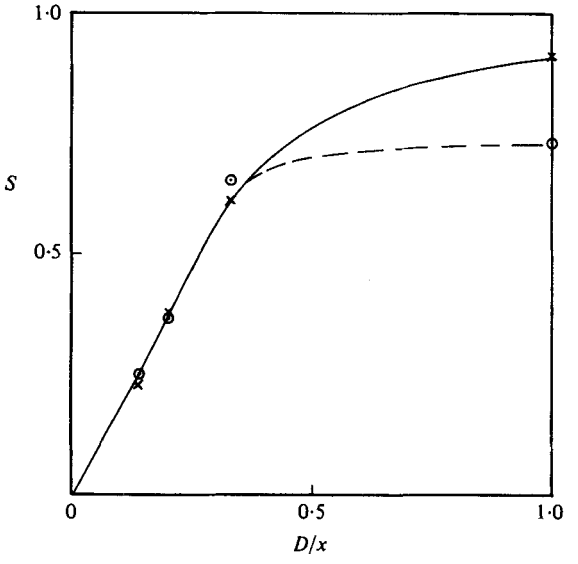

FIGURE 6. Variation of Strouhal number of spectral or coherence maximum withdistance from nozzle. ×, slab schlieren; ⊙, schlieren/near-field-pressure coherence.

the jet velocity, originating in the operation of the compressor, which were of the order of 1 % of that velocity.

Spectra of the schlieren signals obtained with a beam thickness of $\delta = \frac{1}{8}x$ are shown in figure 5. We see that the concentration of high spectral density moves to progressively lower Strouhal numbers as the distance from the nozzle is increased. As discussed in §2, the location of the maximum is not highly sensitive to the sensing-beam thickness and thus reflects a concentration of energy at that Strouhal number owing to the high sensitivity of the schlieren to components with azimuthal coherence. Thus we see that these structures have a streamwise scale which increases with distance from the nozzle. Figure 6 shows that for $x/D > 3$ the peak Strouhal number follows the relation $S = 1{\cdot}8D/x$. At $x/D = 1$ the Strouhal number was appreciably

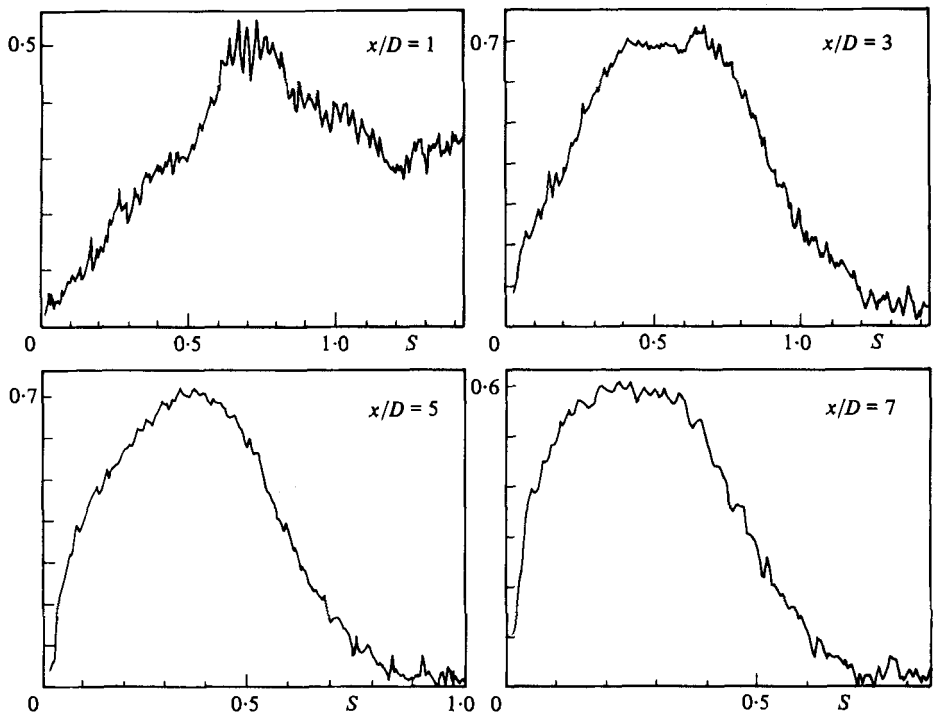

FIGURE 7. Coherence between slab schlieren and near-field pressure. ($\delta = \frac{1}{8}x$; near-field microphone at $y/D = 0{\cdot}5 + 0{\cdot}25x/D$ and in same place as schlieren beam).

less than this value, suggesting that the mechanism for development of the structure in the region very close to the nozzle, where the shear layer would behave in a more two-dimensional manner, is of a different form to that further away (at about 3 nozzle diameters and beyond), where three-dimensional constraints become stronger.

Figure 7 shows the coherence function between the schlieren signal and that of a microphone placed in the near field just outside the shear layer at a distance from the jet axis $y_m/D = 0{\cdot}5 + 0{\cdot}25x/D$ to avoid flow interference with the microphone. The microphone was located at the same distance from the nozzle as the schlieren for the results of figure 7. Cross spectra between schlieren and microphone signals were analysed using a Hewlett Packard 5420A signal analyzer, based on an average of approximately 500 sets of 1000 data samples which were used to determine coherence and phase spectra by Fourier transformation. The coherence reaches a maximum value of approximately 70 %, although this reduces to 50 % at $x/D = 1$ and to 60 % at $x/D = 7$. Thus we see that there is a high degree of coherence between the near-field pressure fluctuations and the azimuthally coherent disturbances in the flow to which the schlieren is sensitive. Again there is a clear trend for the Strouhal number at which peak coherence occurs to decrease with distance from the nozzle, and again the disturbances at $x/D = 1$ show an appreciable departure from the inverse relation which applies beyond $x/D = 3$. The Strouhal numbers for maximum coherence are also plotted on figure 6, and it is seen that they correspond closely with those for maximum spectral energy of the schlieren signals (but not of the microphone signals).

When the schlieren sensing beam and near-field microphone are separated in a streamwise sense, the maximum coherence reduces, as is shown by figure 8(*a*), except

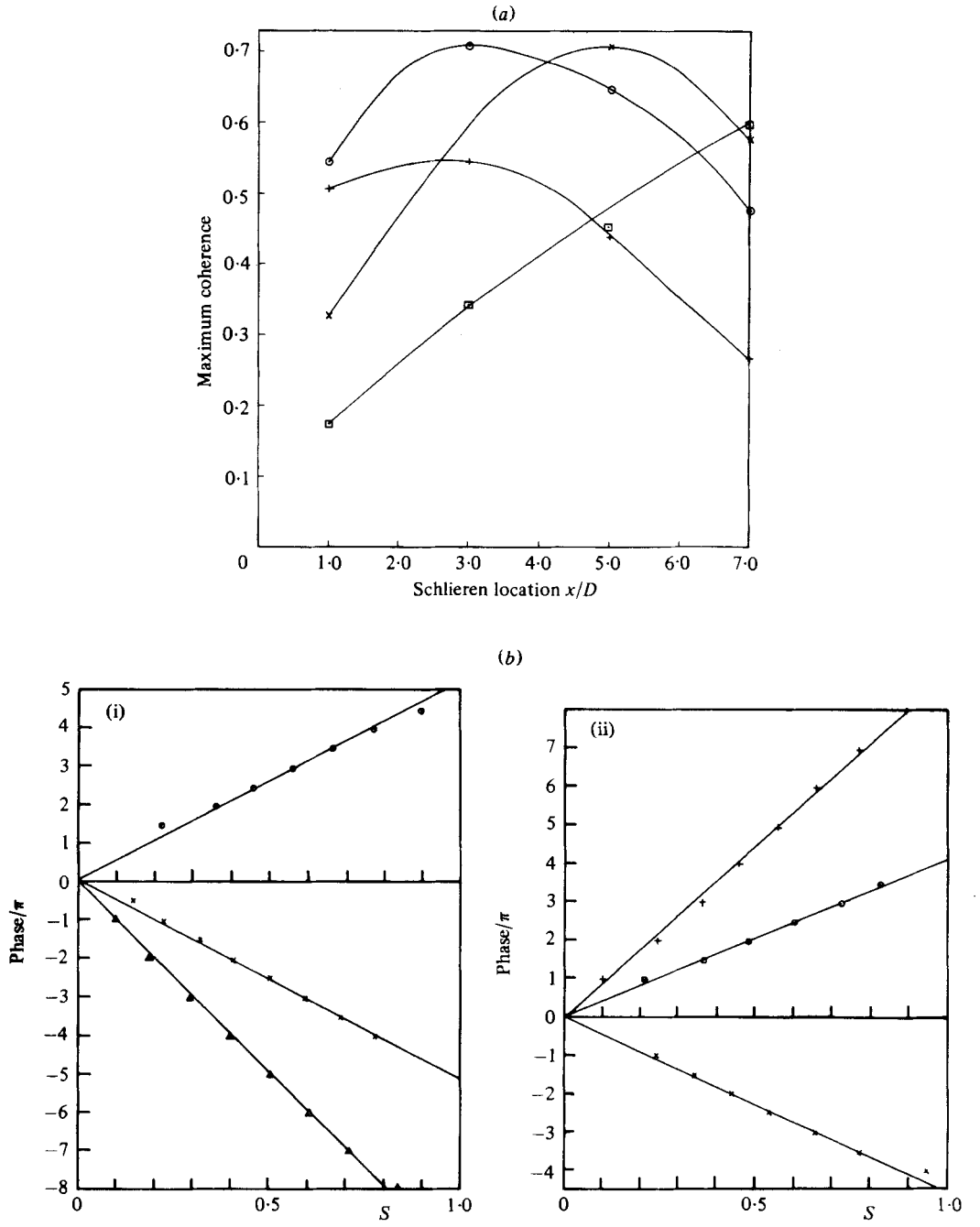

FIGURE 8. (*a*) Variation of maximum coherence between slab schlieren and axially displaced near-field microphone: ⊙, $x_m/D = 3{\cdot}0$; +, 1·0; ×, 5·0; ⊡, 7·0; x_m is distance of microphone from nozzle exit. (*b*) Phase spectra of schlieren and axially displaced near-field microphone: (i) microphone at $x/D = 3$; (ii) microphone at $x/D = 5$; +, $x_s - x_m = 4D$; ×, $-2D$; ⊙, $2D$; △, $-4D$.

that when the microphone is located at $x/D = 1$ it shows a stronger coherence with the flow structure at $x/D = 3$. This result provides an explanation for the unexpectedly low Strouhal numbers at which this maximum coherence occurs (figure 6), and it appears that the near pressure field sensed at $x/D = 1$ is influenced significantly by contributions from further downstream of the nozzle. At greater distances from the nozzle the near-field microphone shows the greatest coherence from the unsteady schlieren signal of the flow adjacent to the microphone. Phase spectra of near-field microphone and displaced-position schlieren signals are shown in figure 8(*b*) and are dominated by the convection with the flow of disturbances between the microphone and schlieren. The convection velocities are quite high, being between 76 % and 96 % of the jet velocity, indicating that the coherent components which predominate in these observations are more closely associated with the inner region of the annular shear layer. Appreciably higher values were observed with the microphone located further from the nozzle, increasing from an average over the different schlieren–microphone separations of $U_c/U_j = 0{\cdot}79$ at $x/D = 1{\cdot}3$ to $0{\cdot}91$ at $x/D = 5$ and to $0{\cdot}96$ at $x/D = 7$. Variations of approximately $\pm 5\,\%$ occurred in the observed convection velocities owing to small positioning errors in the microphone, which was itself of finite size $\frac{1}{4}D$ as was the thickness of the sensing beam. However, there appeared to be no bias dependent upon which of the two sensors was further upstream. This suggests that at positions progressively further from the nozzle exit the near-pressure field is increasingly influenced by the radiation of pressure disturbances from further upstream which would move with the acoustic velocity and propagate either outside or inside the flow, ahead of the components of the originating disturbances in the flow itself. However, as the ambient acoustic velocity exceeds the jet velocity by a factor of 1·5, this effect is certainly not the major feature of the results, which show the convection in the flow of disturbances which are strongly coherent with the near pressure field. Ultimately, as the microphone is moved into the far field the apparent propagation velocity approaches the acoustic velocity, of course.

As the near-field microphone was moved further from the jet axis so the maximum coherence between its signal and that of the flow structure sensed by the schlieren declined steadily from the value of just over 70 % for $y/D = 1{\cdot}75$ shown in figure 7 at $x/D = 5$, to 47 % at $y/D = 2{\cdot}5$, 26 % at $y/D = 4{\cdot}5$ and 7 % at $y/D = 9$. Thus we see that the high coherence observed is essentially a feature of the near pressure field of the flow, and that as the far field is approached so relatively small coherences are observed. In the far field observed at a radial distance of 50 diameters from the nozzle, similarly low values of coherence with the schlieren signals were observed, although both at 45° and 90° to the nozzle axis the peak coherence declined steadily from 11 % for $x/D = 1{\cdot}3$ to 8 % at $x/D = 5$ and to 6 % at $x/D = 7$. Such small values are difficult to measure accurately, even taking 5000 spectral averages, but the phase spectra showed clearly the acoustic time delay for propagation to the far field.

An attempt was made to see whether a greater coherence could be obtained between the flow-structure measurement signal and the far-field pressure by increasing the sensing area of the flow from the rectangular cross-sectional beam of thickness $\frac{1}{8}x$ to a cross-section which extended over $0{\cdot}5 \leqslant x/D \leqslant 7$ and which had sides along $y/D = \pm 0{\cdot}5 + 0{\cdot}25x/D$. Observations were made with the schlieren knife edge sensing axial streamwise density gradients as in the remainder of the observations, and also with the schlieren knife edge set to sense transverse density gradients towards the

far-field microphone when at 90° to the axis, in the hope that thereby some large-scale lateral motion of the jet might be sensed. Coherence between these signals generated over the whole of the first seven diameters of flow and the far field was, however, very small (8 % or less) in all cases, except when the streamwise density gradients were compared with the far field close to the jet axis at 30°, when a maximum coherence of 28 % was observed at $S = 0{\cdot}13$ (figure 9). When compared with a near-field microphone at $x/D = 4$, $y/D = 1{\cdot}5$, much higher coherences were observed, 42 % for the streamwise components and 34 % for the transverse components at $S = 0{\cdot}33$ and 0·41, respectively. In both cases this was a lower coherence than with the schlieren sensing only a smaller slice of thickness $\frac{1}{8}x$ of the flow. Thus the use of this very large sensing aperture over $0{\cdot}5 \leqslant x/D \leqslant 7$ produces a slight decrease of coherence with a near-field microphone, and an appreciable increase of coherence with a far-field microphone near the downstream axis, although in the latter case the coherence is still not very large. These results again indicate that the near pressure field is dominated by adjacent coherent disturbances in the flow and that inclusion of zones further upstream and downstream merely introduces effects less coherent with the near field and reduces the overall coherence from about 70 % to about 40 %. The increased coherence with the far field occurs at a low Strouhal number, showing that the much larger schlieren aperture has made it more responsive to very-large-scale disturbances as discussed in § 2 and that it is for these large-scale components that increased coherence with the far field occurs.

Using the chevron-shaped aperture (figure 1*b*) the coherence between the schlieren signal and near-field pressure of adjacent microphones at $x/D = 2$, 4 remained at just below 70 % when the centre of the apex of the chevron cross-section beam intercepted the jet axis at $x/D = 4$, and was found to be virtually independent of the chevron thickness as this was varied between $\frac{1}{8}D$ and $\frac{3}{8}D$. Coherence between the chevron cross-section beam and the far-field pressure was again small at about 6 %. Thus it appears that the use of this particular beam geometry is not effective in producing any further enhancement of coherent flow effects beyond that which can be obtained with the rectangular cross-section beam. The chevron shape was selected because some of the disturbances suggested by the visual observations of Crowe & Champagne (1971) and Moore (1977) gave the impression of such a shape in the structure. Clearly, more accurate matching of the sensing aperture to the structure would be needed to produce a significant change in observed responses.

The pressure fluctuations inside the potential core of the jet were observed using a microphone mounted on a sting supported within the contraction and extending downstream to the nozzle along the centre line of the nozzle. This avoided having any of the microphone support structure interacting with the turbulent mixing region of the jet. The microphone was a standard Bruel and Kjaer 3 mm diameter type with a sharp pointed fairing and annular gauze vent, the fairing providing a curved after-body of total length approximately 6 mm beyond the microphone face. When the microphone was located with its vent and sensing face in the plane of the main 12·7 mm diameter flow nozzle, the spectra of the schlieren signals at various positions were found to be virtually identical to those of figure 5 in form and it appeared that insertion of the microphone to this position had not interfered appreciably with the flow. In particular, it did not seem that any wake from the microphone casing and its curved after-body fairing had contributed to the flow disturbances.

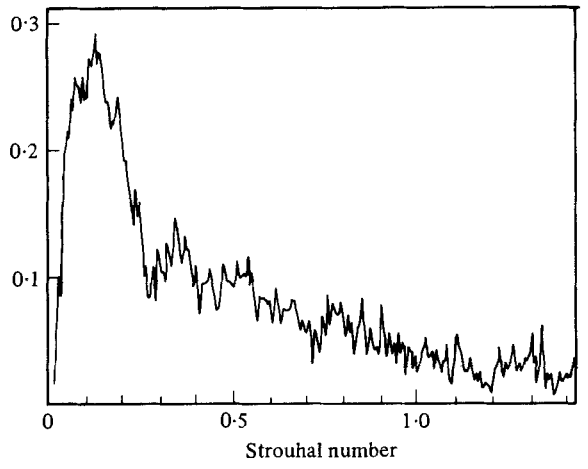

FIGURE 9. Coherence between schlieren sensing whole jet ($0{\cdot}5 < x/D \leqslant 7$) and far-field microphone at 30° to jet axis (schlieren sensitive to axial deflections of beam).

The inside pressure field of the potential core at the nozzle exit showed coherence with the flow structure over a much narrower range of Strouhal number than did the near-field pressure field outside the shear layer, as shown by figure 10(*a*). Appreciable coherence exists only over $0{\cdot}6 < S < 1{\cdot}04$ and decreases from a maximum of 50 % to 24 % as the flow is sensed at distances increasing from 1 to 6 diameters downstream, showing that the pressure field inside the potential core at the nozzle exit is due primarily to a more limited range of flow disturbances than is the near field outside the shear layer. As the jet was operated at a Mach number of 0·7 it is likely that the flow causes appreciable refractive effects which largely prevent propagation from downstream back to the nozzle. The apparent convection speed of the flow disturbances which were coherent with the pressure at the exit plane increased steadily from $0{\cdot}46U_j$, when the jet schlieren was displaced to $x/D = 1$, to $0{\cdot}78U_j$ when the schlieren was located at $x/D = 6$. This steady increase of apparent velocity combined with the steady decline in coherence indicates that the disturbances which produce the exit-plane pressure fluctuations become more concentrated towards the inner high-velocity side of the mixing shear layer as they decay and move downstream.

When the microphone mounted on the sting support was moved to a position where its sensing face lay at $x/D = 2$, it was found that a set of distinctive disturbances was introduced to the flow. This is shown in figure 10(*b*) where the schlieren–microphone coherence is plotted, although the same set of components was equally clearly evident in the microphone and schlieren spectra as well as in the co-spectral density function, the latter tending to show the components most sharply defined. Phase spectra between the fixed microphone and the schlieren at different positions show slight oscillations corresponding to the peaks in coherence, but these were quite small and the motion of the entire structure had an apparent velocity of between 80 % and 90 % of the jet velocity, this tending to increase as the schlieren was moved further downstream. Since the results shown with the microphone at $x/D = 0$ did not show any of these strong relatively discrete effects, it appears that the physical presence of the centre body in the potential core of the jet has provided an additional physical constraint to the jet as a whole so that very regular disturbances are produced

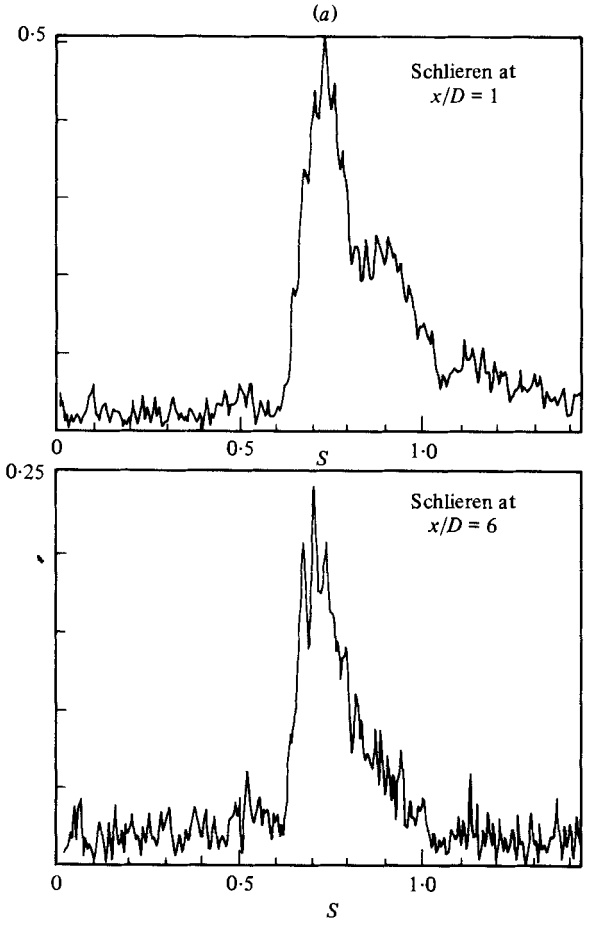

FIGURE 10 (*a*). For legend see page 48.

within its initial mixing layer. These disturbances are still evident six diameters away from the nozzle, although much weaker there in relation to the natural structure of the jet. The natural structure of the jet is evident in the underlying broadly distributed coherence between microphone and schlieren, which moves to a lower Strouhal number as the schlieren is moved downstream. In this respect, the unsteady pressure field at $x/D = 2$ in the potential core appears quite distinct from that at the nozzle exit plane, where it remained coherent with the downstream structure at fixed (and over a relatively narrow range of) Strouhal numbers (figure 10*a*). This may be attributed to the relatively high Mach number at which these observations were made, tending to prevent the potential core-pressure fluctuation at the nozzle exit experiencing the same interrelation with the downstream flow field owing to acoustic refraction effects as do the near-field pressure outside the flow and the potential core pressure further downstream (i.e. $x/D = 2$ in these observations).

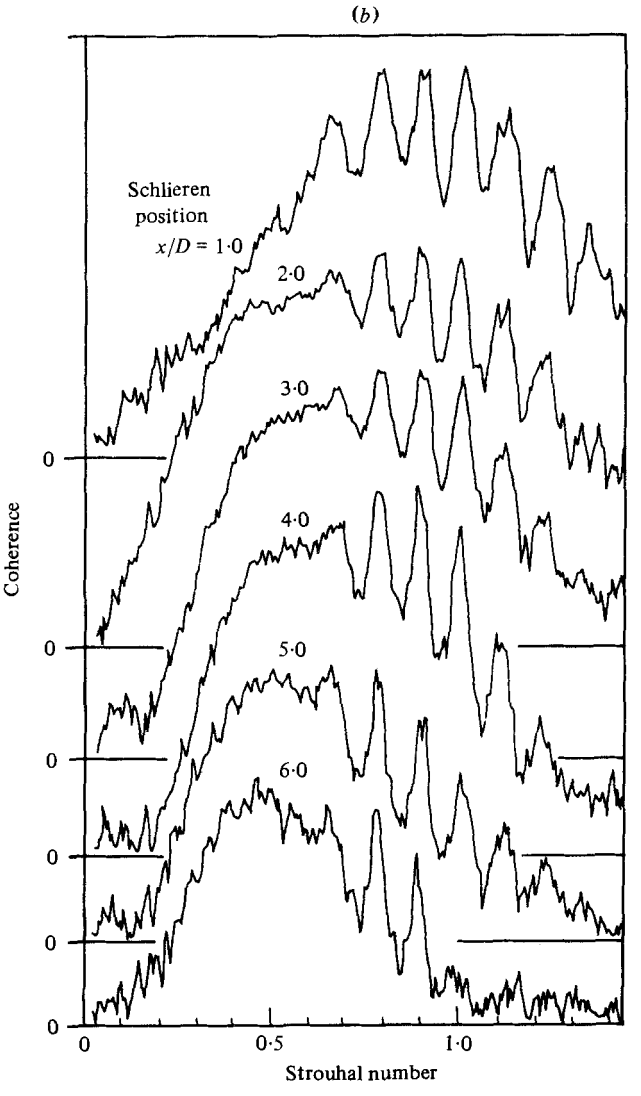

FIGURE 10. Coherence between slab schlieren and central microphone at (*a*) $x_m/D = 0$, (*b*) $x_m/D = 2$; $\delta = \frac{1}{8}x_s$.

3.2. *The harmonically excited jet*

The ultrasonic horn mounted in the plenum chamber (figure 1*b*) excited the jet at a Strouhal number of 1·12 and produced in the nozzle exit plane a sound-pressure level of 124·5 dB. At the jet-operating Mach number of 0·7 this corresponds to a true peak induced-velocity fluctuation of 0·56 % of the mean-flow velocity. It was found that, with the acoustic excitation on, the overall intensity of the flow-structure disturbances decreased as shown in figure 11(*a*). The corresponding changes in spectral density are shown in figure 11(*b*), these being corrected to eliminate small contributions due to the combination of the strong discrete component and the 6 % filter characteristic. It is seen that reductions in spectral density of around 70 % occur at $S = 0{\cdot}75$, midway between the excitation frequency and half that frequency, whilst

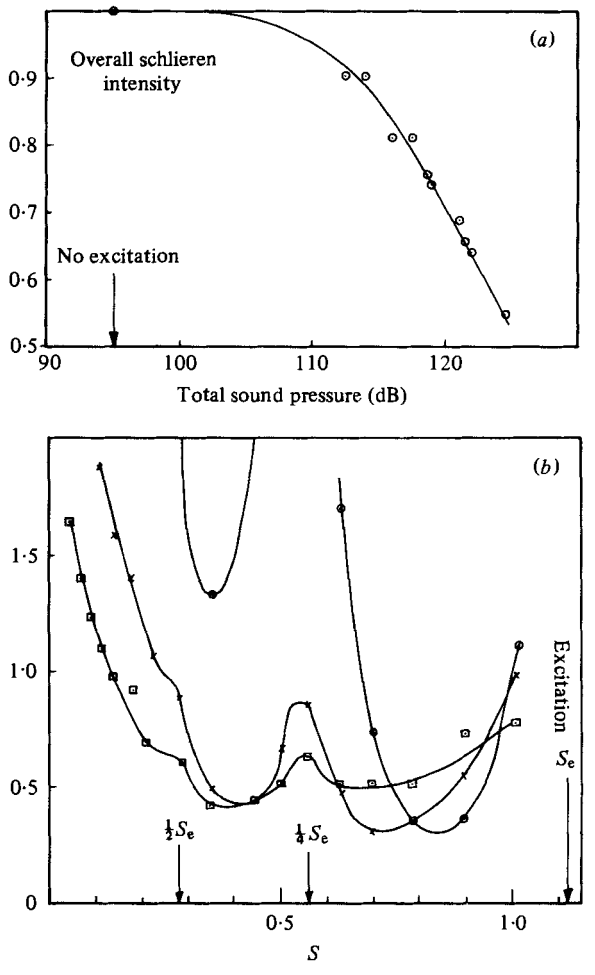

FIGURE 11. (*a*) Reduction of overall slab schlieren intensity with increasing harmonic excitation ($x_s/D = 4$, $\delta/D = 0{\cdot}5$, sound pressure measured at $x_m/D = 1$, $y_m/D = 0{\cdot}75$, vertical scale is relative intensity). (*b*) Relative change in slab schlieren spectral density owing to application of harmonic excitation (spectral density with excitation/that without excitation). $\delta = \frac{1}{8}x_s$, results from 6 % filtered spectra. ×, $x_s/D = 4$; □, 6; ⊙, 2; large peaks at $S = 0{\cdot}56$, $0{\cdot}28$ are off scale.

the spectral changes also show evidence for half- and quarter-frequency components being introduced. Thus it appears that the excitation has had the effect of concentrating the flow-structure disturbances into specific bands, depleting bands in between. Small reductions in far-field noise of approximately 1 dB were also observed at frequencies intermediate between the excitation and its subharmonics. Moore (1977) has also observed similar far-field sound effects, but notes that the broad-band sound is increased when exciting at smaller Strouhal numbers, with a maximum at about 0·3, and that small reductions are only obtained with the higher-Strouhal-number excitation.

The coherence between the flow-structure signal observed with an $\frac{1}{8}x$ thickness beam and the adjacent near-field pressure is shown in figure 12(*b*) whilst the schlieren energy spectra themselves are shown in figure 12(*a*). The vortex-pairing mechanism

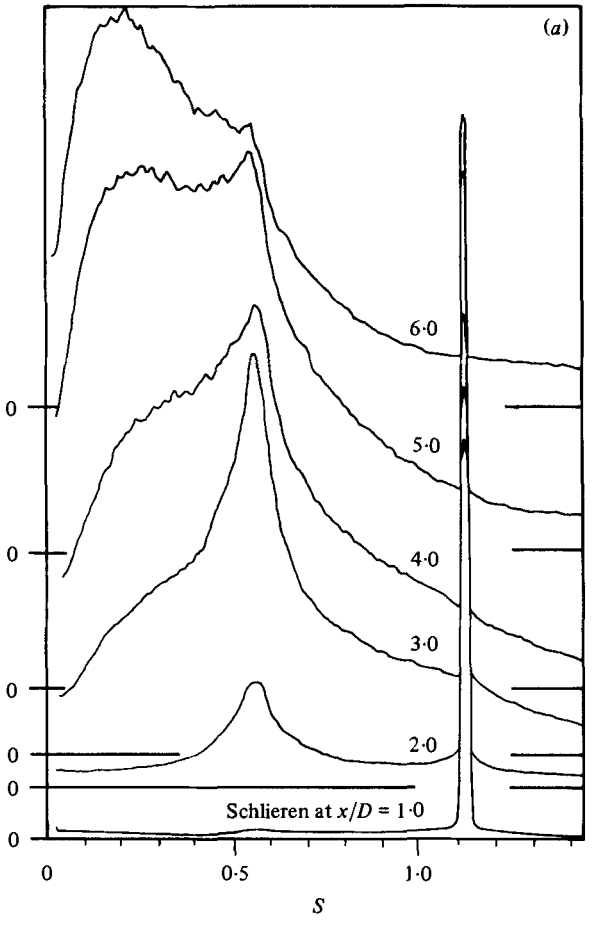

FIGURE 12(*a*). For legend see facing page.

is quite clear in the energy spectra, the first subharmonic of the excitation developing at $x/D = 3$ and the second at $x/D = 6$. These distances are appreciably further from the nozzle than previous demonstrations at similar Reynolds numbers of the pairing mechanism (see e.g. Davies & Yule 1975) and detection of the mechanism at these positions is attributed to the enhancement of azimuthally coherent components by the schlieren system. Coherence at the first subharmonic was maintained over a relatively long distance between $x/D = 1$ and $x/D = 4$ at between 0·45 and 0·55, whilst the coherence at the second subharmonic rose to 0·45 at $x/D = 6$. The energy spectra, however, show more clearly the growth in strength of the first subharmonic until it greatly exceeds the excitation at $x/D = 3$, and similarly a growth in the strength of the second subharmonic at $x/D = 6$. The disturbances at the excitation frequency can be clearly identified over the whole range of observation positions, although they carry a steadily declining fraction of the total energy as distance from the nozzle exit increases. Once again, phase spectra of separated near-field microphone and schlieren beams showed a relatively high convection velocity between 0·75 and 0·85 of the jet velocity.

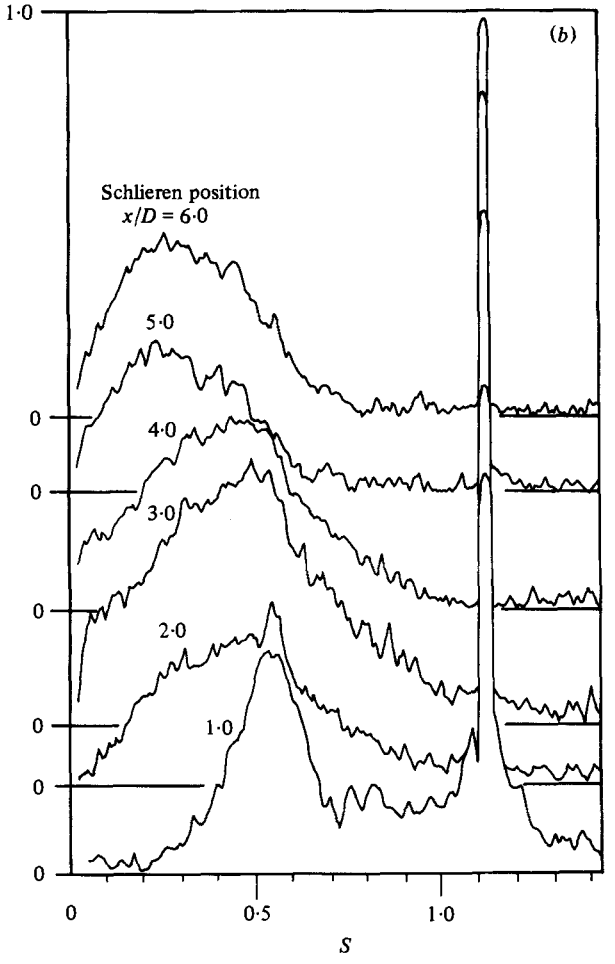

FIGURE 12. (*a*) Slab schlieren spectra under harmonic excitation (vertical scale is spectral density, linear scale, $\delta = \frac{1}{8}x_s$, zero datum for each spectrum is different, as marked). (*b*) Coherence between slab schlieren and near-field microphone under harmonic excitation (microphone in same place as schlieren beam at $y_m/D = 0{\cdot}5 + 0{\cdot}25x_m/D$).

3.3. *The impulsively excited jet*

The response of a microphone and of the schlieren beam to the impulse produced by the spark gap (figure 1*a*) is shown in figure 13. The microphone signal corresponds in amplitude to an acoustic disturbance having a velocity range of approx. 20 % of the jet velocity, so it is clear that the impulse will produce a strong perturbation of the jet. Although the pressure impulse is not very simple in form, it is relatively compact and comprises two main compressions interspaced by somewhat broader expansions, the interval between the compressions being 60 μs or a time corresponding to a flow movement of $U\delta t/D = 1{\cdot}1$. The form of this pulse corresponds closely with that expected for an N-wave from a spark incident upon an orifice (Blackstock 1980). Small echo effects were noted at times after the initial impulse, these being less than 10 % of the initial impulse at $U\delta t/D = 6$ and less than 3 % of the initial disturbance at $U\delta t/D = 12$, approximately. The intervening periods contained almost no disturbances,

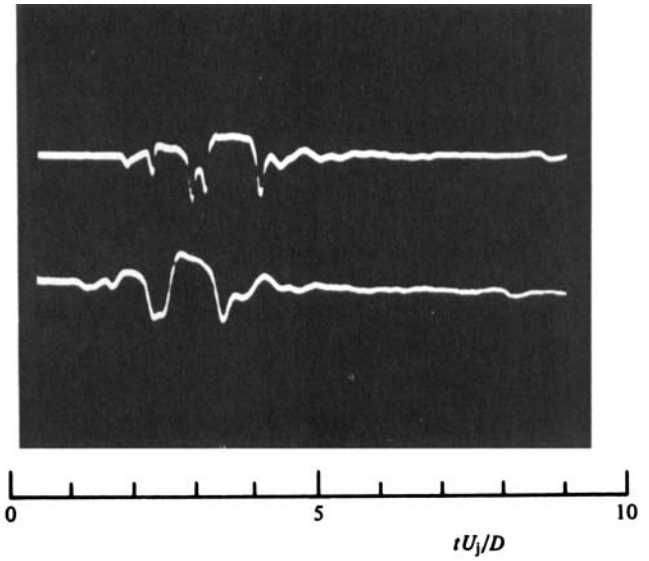

FIGURE 13. Impulse excitation response with no flow (observed outside nozzle). Upper trace: microphone, $x_m/D = 3$. Lower trace: schlieren, $x_s/D = 2$, $\delta = \frac{1}{4}D$.

as figure 13 shows. Thus we see that the excitation comprised a relatively compact impulse having two strong, sharp compressions separated by longer expansion. Heavens (1978) has presented a series of schlieren photographs of the disturbance produced by the spark source as it moves away from the nozzle, and it appears to comprise a single strong perturbation of the flow.

Microphone and schlieren signals were recorded using a beam thickness of $\frac{1}{8}x$. In addition, a photocell recorded a trigger pulse on the recording tape directly from the light impulse of the spark so as to provide an accurate relative time origin on the recordings. Typical time responses averaged over approximately 600 impulses are shown in figure 14. A short section of the unexcited traces appears as a straight line at the left end ($t < 0$) of each record. These sections showed negligible amplitude compared with the excited portion of the record. The initial acoustical impulse is more clearly evident in the microphone-averaged responses, and the time scales of the traces have all been adjusted for zero time at the commencement of this initial pressure wave. The first large flow disturbance follows this excitation pulse with a delay time which increases with distance from the nozzle, corresponding to the motion of the flow disturbance at the lower convection speed of the flow. The most interesting feature of the responses is the length of time over which they persist. At three or four diameters from the nozzle there was still slight evidence of the transient at $t = 400D/U_j$, whilst the amplitude at $t = 200D/U_j$ remained as much as 20 % of the maximum disturbance in the schlieren response. Compared with the excitation shown in figure 13 it is clear

FIGURE 14. Impulse time-average response with flow. (*a*) Microphone at $y_m/D = 0{\cdot}5 + 0{\cdot}25x/D$. (*b*) Schlieren slab beam, $\delta = \frac{1}{8}x$. Horizontal scales show tU_j/D. Upper traces at $x/D = 1$, centre at $x/D = 3$, lower at $x/D = 5$. Vertical scales in arbitrary units (initial microphone signal at $tU_j/D = 0$ corresponds to initial pressure wave producing approx. $0{\cdot}2U_j$ velocity perturbation).

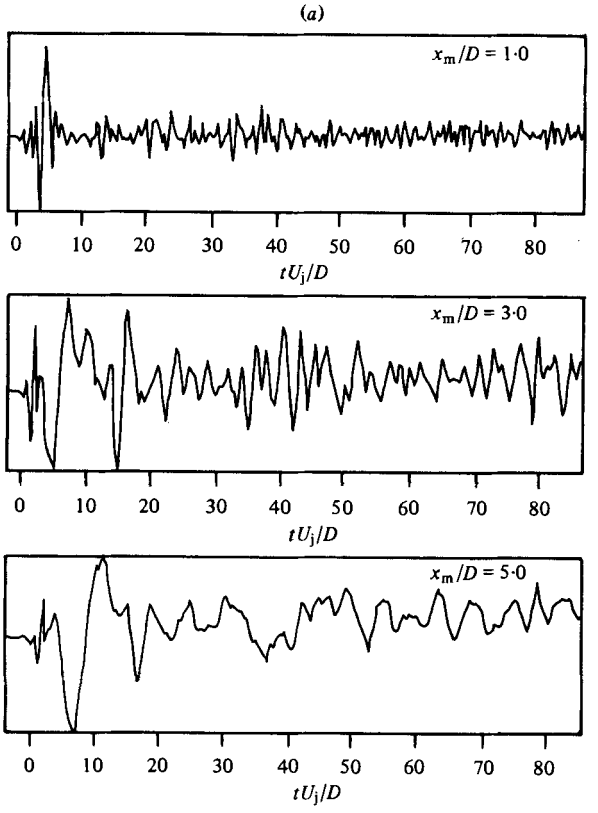
(a)
$x_m/D = 1{\cdot}0$
0 10 20 30 40 50 60 70 80
tU_j/D
$x_m/D = 3{\cdot}0$
0 10 20 30 40 50 60 70 80
tU_j/D
$x_m/D = 5{\cdot}0$
0 10 20 30 40 50 60 70 80
tU_j/D

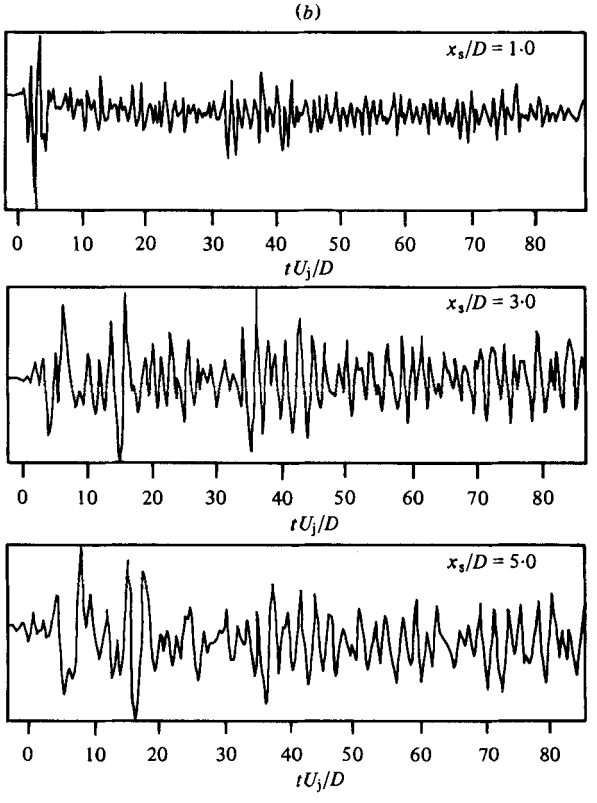
(b)
$x_s/D = 1{\cdot}0$
0 10 20 30 40 50 60 70 80
tU_j/D
$x_s/D = 3{\cdot}0$
0 10 20 30 40 50 60 70 80
tU_j/D
$x_s/D = 5{\cdot}0$
0 10 20 30 40 50 60 70 80
tU_j/D

that the presence of the flow has introduced a strongly resonant effect which persists for relatively very long times after the initial excitation pulse has passed. Even the small echoes of the initial pressure pulse noted with no flow do not explain the persistence of the transient, as they occur at relatively short times after the initial disturbance ($t = 6D/U_j$ and $12D/U_j$ as discussed above).

The long duration of the transient response made it possible to examine its spectral content on the basis of signal samples taken during the transient. Spectral averages were formed over approximately 1300 sets of signal samples taken at varying times after the initial transient had passed. The overall time length of each individual set of sampled values was approximately $200D/U_j$, during which time 1000 samples were recorded. The initial time of the first signal sample after the initial transient was varied between zero and $10D/U_j$ over six values in accumulating the 1300 transforms from approximately 200 actual impulse records. It was found that both microphone and schlieren spectra showed the presence of a number of discrete components, some being quite closely spaced and thus related to a slight beating effect observable in the time-average responses. The discrete components were not particularly evident in the coherence function and it thus appears that they have a similar coherence to the broad-band disturbances of the natural jet upon which the excitation was superimposed. The clearest resolution of the spectral content of the transient response was obtained in the schlieren/microphone co-spectral density function which is shown in figure 15. It may be seen that a number of discrete components are stimulated during the transient and that these may be identified at a number of different distances downstream of the nozzle. However, as the streamwise distance from the nozzle is increased, so the relative strength of these components changes, the lower-Strouhal-number components being stronger further away from the nozzle.

The extremely long time over which the transient persisted and its relatively large number of discrete spectral components were not thought to be due to the acoustic behaviour of the plenum chamber. This had a Helmholtz type of resonance at approximately 100 Hz, which corresponds to a period of $1800D/U_j$, this being about ten times the transient duration. Also the observed response with no flow showed a relatively short-duration excitation disturbance (figure 13) which did not appear to show any ringing after this initial disturbance. As discussed, weak echoes were observed in the no-flow excitation, and did not suggest that the excitation was the cause of the long duration of the transient response unless the jet were proportionately highly sensitive to extremely weak echoes not observed in the no-flow excitation records. Further, the response is shown by figure 15 to be strongly dependent upon distance from the nozzle, demonstrating directly the influence of the mixing jet flow on the impulse observed. It is concluded that the flow in the jet had played a major role in producing the long-duration transient with a complex spectral composition dependent upon distance from the nozzle.

The sharp peaks in the spectra of figure 15 were not caused by taking insufficient spectrum averages, but were a genuine feature of the responses as discussed. Whilst the response is certainly flow-related, as shown by the variation with distance from the nozzle, it remains a possibility that the particular spectral components excited are caused by very weak diffraction or resonant effects associated with the nozzle, spark and plenum chamber and which could not be observed (figure 13) but which produced a significant response owing to nonlinear effects. A further detailed investi-

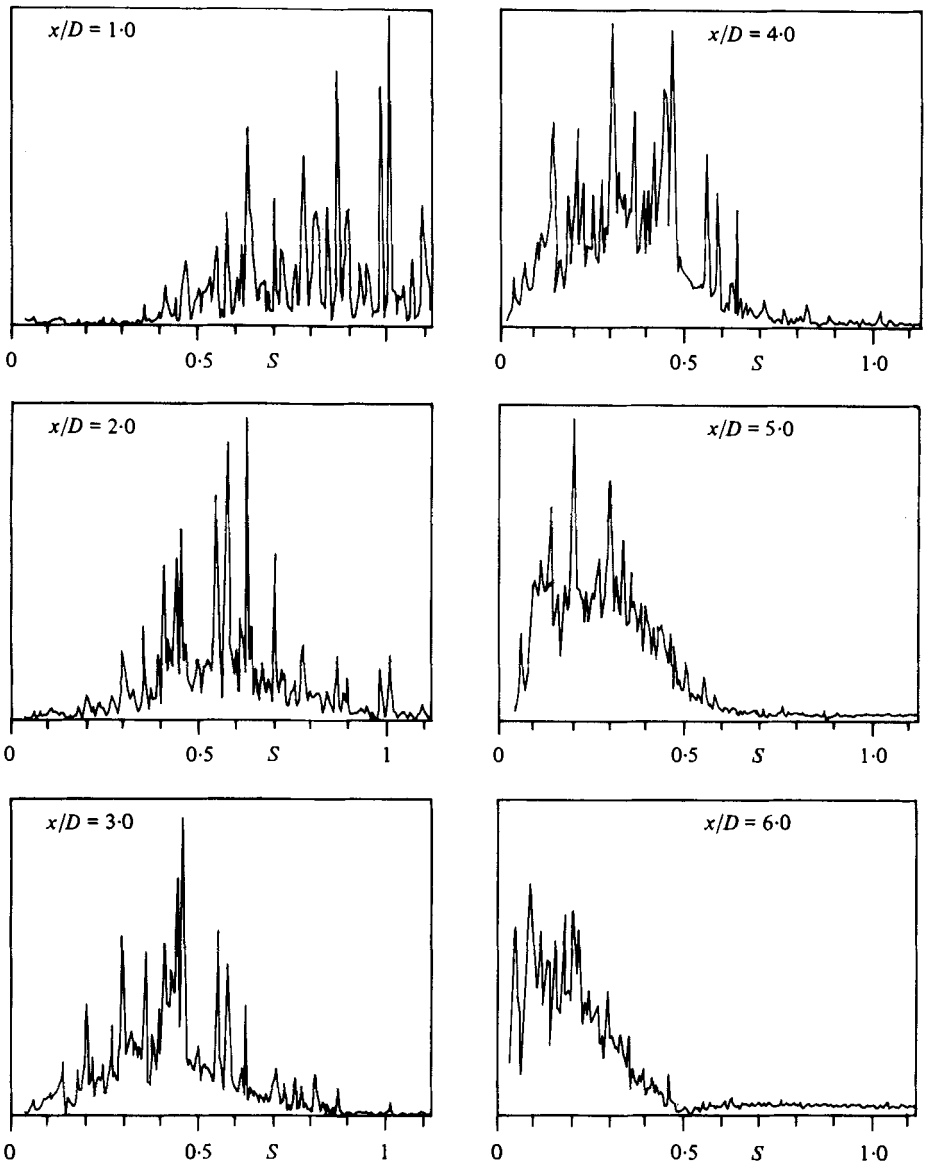

FIGURE 15. Microphone–schlieren co-spectral density during impulse transient (microphone in plane of schlieren beam). Vertical scales show co-spectral density (arbitrary units, same scale).

gation (using a completely revised system excited by a shock wave instead of a spark, and an acoustically treated plenum) is being planned to determine whether the particular set of discrete components observed is inherent to the mixing flow or to system-dependent effects combined with a very nonlinear response.

4. Conclusions

By sensing the total fluctuation over a complete cross-section of the flow, components of the flow structure which have azimuthal coherence are strongly emphasized. In a natural jet these occur at a Strouhal number which decreases inversely with

	Excited jet x/D						Natural jet centre-body interference
	1	2	3	4	5	6	$1 \leqslant x/D \leqslant 6$
Impulse response	—	—	—	—	—	0·09†	—
	—	—	—	0·14	0·14	—	—
	—	—	—	—	—	0·18	—
	—	—	0·20	0·20	0·20†	0·20	—
	—	—	0·30	0·29†	0·30	—	—
	—	0·36	0·36	—	—	—	—
	—	0·41	0·41	—	—	—	—
	—	0·44	0·44	0·43	—	—	—
	—	0·45	0·45†	0·45	—	—	—
	—	0·54	0·55	0·55	0·55	—	—
	0·57	0·57	0·58	0·60	—	—	—
	0·62	0·62†	0·62	0·63	—	—	0·65
	0·70	0·70	—	—	—	—	—
	0·78	0·78	—	—	—	—	0·78
	0·87	0·87	—	—	—	—	0·90
	0·98	—	—	—	—	—	—
	1·01†	1·01	—	—	—	—	1·00
	1·09	—	—	—	—	—	1·11
							1·23
							1·33
Harmonic response	—	—	0·55	—	—	0·26	
Natural jet maximum coherence	0·91	0·75	0·61	0·47	0·37	0·25	—

TABLE 1. Comparison of Strouhal numbers identified. The last column refers to results of figure 10(*b*) and similar observations at other positions in the flow with the centre body fixed at $x_m/D = 2$. † denotes the strongest component in the response.

distance from the nozzle, and at a substantially higher Strouhal number for maximum spectral energy than the near pressure field. Coherence with the near pressure field in excess of 70 % was observed at the Strouhal number where the spectral maximum reflects high azimuthal coherence. Convection of the large-scale structures occurs at a relatively high velocity, values of between 75 % and 95 % of the jet exit velocity being obtained, showing these to be more closely associated with the inner edge of the mixing layer. A reduced coherence existed between the pressure field in the potential core at the nozzle exit plane and the flow structure sensed further away, and it appears that the relatively high Mach number of the flow has introduced refraction effects which prevent the flow structure influencing the pressure field at the exit plane. Introduction of the microphone casing protruding to $x/D = 2{\cdot}5$ from the nozzle led to the occurrence of a set of strong discrete components in the range $0{\cdot}65 < S < 1{\cdot}33$. These had almost completely died away in the flow at $x/D = 6$ and are thus associated with the interaction of the annular shear layer with a solid centre body.

Pure-tone excitation of the jet at $S = 1{\cdot}12$ progressively reduced the intensity of the observed mixing structure and also produced small reductions in the far-field noise. It gave rise to strong subharmonic components at $S = 0{\cdot}55$ and $0{\cdot}26$ which were most strongly coherent with the near pressure field at $x/D = 3$ and 6, respectively. As table 1 shows, the natural jet experiences a progressive change in maximum Strouhal number of the turbulence with distance along the axis, whilst the har-

monically excited jet showed only distinct Strouhal numbers in an approximately halving sequence. Under impulse excitation a response containing a number of discrete spectral components (depending upon x/D) was observed and the transient was found to decay over a relatively long period of time. The strongest component of the impulse response decreased in Strouhal number with distance more rapidly than that in the harmonically excited or natural jet cases, the latter being quite similar. Also the impulse response shows a much larger number of components in its response. It seems likely that one contributing factor to these differences in response is that the impulse excitation was relatively much stronger.

The work described in this paper was carried out whilst the author was at the Whittle Turbomachinery Laboratory, Engineering Department, Cambridge University. The support of the Science Research Council and of Professor J. E. Ffowcs Williams is gratefully acknowledged. Mr N. Eshelby provided valuable assistance with the experimental work.

REFERENCES

BLACKSTOCK, D. T., WRIGHT, W. M., LOCKWOOD, J. C., CORNET, E. P., ANDERSON, M. O., KLEEMAN, D. R., COBB, W. N., ESSERT, R. D. & DAVY, B. A. 1980 Non-linear acoustics illustrated by experiments with N-waves produced by sparks. In *Proc. 10th Int. Acoustics Cong.*, Sydney, vol. 1, p. 160.

BRADSHAW, P., FERRIS, D. H. & JOHNSON, R. F. 1964 Turbulence in the noise-producing region of a circular jet. *J. Fluid Mech.* **19**, 591–624.

BROWN, G. L. & ROSHKO, A. 1974 On density effects and large structures in turbulent mixing layers. *J. Fluid Mech.* **64**, 775–816.

BRUUN, H. H. 1977 Time-domain analysis of the large-scale flow structure in a circular jet. Part 1. Moderate Reynolds number. *J. Fluid Mech.* **83**, 641–671.

CROW, S. & CHAMPAGNE, F. H. 1971 Orderly structure in jet turbulence. *J. Fluid Mech.* **48**, 547–591.

DAVIES, P. O. A. L. & YULE, A. J. 1975 Coherent structures in turbulence. *J. Fluid Mech.* **71**, 317–338.

DAVIS, M. R. 1971 Measurement in a subsonic turbulent jet using a quantitative schlieren system. *J. Fluid Mech.* **46**, 631–656.

DAVIS, M. R. 1972 Quantitative schlieren measurements in a supersonic turbulent jet. *J. Fluid Mech.* **51**, 435–447.

DAVIS, M. R. 1975 Intensity, scale and convection of turbulent density fluctuations. *J. Fluid Mech.* **70**, 463–479.

DAVIS, M. R. & DAVIES, P. O. A. L. 1979 Shear fluctuations in a turbulent jet shear layer. *J. Fluid Mech.* **93**, 281–305.

HEAVENS, S. N. 1978 Visualization of unsteady jets and aerodynamic noise fields. In *Proc. 13th Int. Cong. on High-Speed Photography and Photonics*, Tokyo.

MOORE, C. J. 1977 The role of shear-layer instability in jet exhaust noise. *J. Fluid Mech.* **80**, 321–368.

TOWNSEND, A. A. 1979 Flow patterns of large eddies in a wake and in a boundary layer. *J. Fluid Mech.* **95**, 515–537.

WIDNALL, S. E., BLISS, D. B. & TSAI, C. Y. 1974 The instability of short waves on a vortex ring. *J. Fluid Mech.* **66**, 35–47.

WINANT, C. D. & BROWAND, F. K. 1974 Vortex pairing: the mechanism of turbulent mixing-layer growth at moderate Reynolds number. *J. Fluid Mech.* **63**, 237–255.

WINARTO, H. 1979 Turbulent density structures of jets and flames. Doctoral thesis, University of New South Wales.